

## Polarization dependence and surface sensitivity of linear and nonlinear photoemission from Bi/Cu(111)

A. Akin Ünal,<sup>1</sup> Aimo Winkelmann,<sup>1</sup> Christian Tusche,<sup>1</sup> Francesco Bisio,<sup>2</sup> Martin Ellguth,<sup>1</sup> Cheng-Tien Chiang,<sup>1</sup> Jürgen Henk,<sup>3</sup> and Jürgen Kirschner<sup>1</sup>

<sup>1</sup>Max Planck Institute of Microstructure Physics, Weinberg 2, 06120 Halle, Germany

<sup>2</sup>CNR-SPIN, Corso Perrone 24, I-16152 Genova, Italy

<sup>3</sup>Institut für Physik-Theoretische Physik, Martin-Luther-Universität Halle-Wittenberg, 06099 Halle, Germany

(Received 6 July 2012; revised manuscript received 31 August 2012; published 27 September 2012)

We analyze the polarization dependence of photoelectron momentum maps observed in one-photon photoemission (1PPE) and two-photon photoemission (2PPE) from clean Cu(111) surfaces and from surface alloys of Bi on Cu(111). For clean Cu(111), we find similar emission patterns and a similar polarization dependence in 1PPE and 2PPE due to the dominating influence of direct optical transitions between initial and final *bulk* states. In contrast, on the Bi/Cu(111) surface, we observe significantly different emission patterns between linear and nonlinear photoemission measurements. This behavior is assigned to the presence of unoccupied states, which favor *surface* two-photon transitions specific to the Bi surface alloy and suppress the strong bulk contribution seen in 1PPE. The polarization dependence of the 2PPE momentum patterns can be assigned to the properties of the occupied states of the Bi/Cu(111) surface alloy, which we analyze with the help of one-step photoemission calculations.

DOI: 10.1103/PhysRevB.86.125447

PACS number(s): 73.20.-r, 79.60.-i

### I. INTRODUCTION

Angle-resolved photoemission spectroscopy (ARPES) is a powerful tool to investigate the electronic structure of materials.<sup>1,2</sup> The symmetry character of the electronic states probed by ARPES manifests itself in the sensitivity of the photoemission matrix element to the polarization vector of the incident light. For example, optical selection rules are enforced by the symmetry of both the initial and the final states in photoemission, which is extremely useful for the qualitative interpretation of measurements in high-symmetry directions of crystals.<sup>3,4</sup> For the quantitative interpretation of photoemission intensities, however, one has to rely on theoretical calculations to reveal the specific sensitivity of the photoemission signal to the polarization of the excitation light. Compared to the linear one-photon photoemission process on which conventional ARPES is based, additional possibilities are provided by nonlinear multiphoton photoemission, which is sensitive to intermediate unoccupied states. Compared to polarization-dependent ARPES, however, the polarization dependence of momentum-resolved multiphoton photoemission has been studied much less.

In this paper, we use a combination of a femtosecond-laser-based photoemission light source coupled with a *momentum microscope*<sup>5,6</sup> to compare the polarization dependence of linear [one-photon photoemission (1PPE)] and nonlinear (multiphoton) photoemission at Cu(111) and Bi/Cu(111) surfaces. The momentum microscope is especially suited for such polarization-dependent investigations because it makes possible the collection of the photoelectrons in the complete half-space above a crystal surface without mechanical movement of neither the sample nor the detection stage, thus, ensuring that all changes observed in the  $k_{\parallel}$ -dependent electron intensity are due to changes in the incident light only. The momentum microscope provides an efficient and direct mapping of all the photoelectron  $k$  vectors parallel to the surface and, thus, enables us to conveniently analyze

effects related to the symmetry of the surface electronic structure and the polarization dependence in the  $k$ -resolved optical transitions extending beyond high-symmetry directions in  $k_{\parallel}$  space. A laser-based light source<sup>7-9</sup> is especially well suited to the momentum microscope as the focus can be efficiently confined to the specific sample region, which is subsequently analyzed by the electron optics, thus, providing optimal brilliance.

Surface alloys of Bi and other heavy elements on fcc(111) surfaces have attracted great interest as model systems for the study of spin-split electronic states in nonmagnetic systems.<sup>10,11</sup> Figure 1 shows a comparison of linear and nonlinear photoemission processes in the electronic structure of Bi surface alloys near the  $\bar{\Gamma}$  point at the Cu(111) surface.<sup>12,13</sup> The schematic spin-orbit-influenced Rashba-type dispersion shown in Fig. 1 is a rather general feature of Bi, Pb, and Sb surface structures on Cu(111) and Ag(111) surfaces with correspondingly different Fermi levels and bulk band gaps.<sup>10,14-16</sup> As shown by the black vertical arrows, 1PPE exclusively probes the occupied surface and bulk states. In comparison, two-photon photoemission (2PPE) can also probe the same occupied states and the unoccupied states as shown by the blue vertical arrows. For Cu(111), the Bi-induced surface states of the  $sp_z$  and  $p_x p_y$  characters with negative effective masses show band maxima at  $E_1 = 0.1$  and  $E_2 = 1.4$  eV, respectively. These bands replace the Shockley surface state of clean Cu(111) and accommodate the  $p$  electrons donated by the bismuth atoms. The maxima of the Rashba parabolas are symmetrically shifted away from the  $\bar{\Gamma}$  point by  $k_{\text{offset}} = \pm 0.04$  and  $\pm 0.05 \text{ \AA}^{-1}$  for  $sp_z$  and  $p_x p_y$  surface states, respectively. We have shown previously that the unoccupied  $p_x p_y$  states of the Bi surface alloy can be experimentally identified in 2PPE measurements.<sup>12</sup> Because these unoccupied Bi states populate the Cu(111) bulk band gap, they lead to additional optical transitions in 2PPE as compared to 1PPE. As we show, this is the reason why we observe drastically different

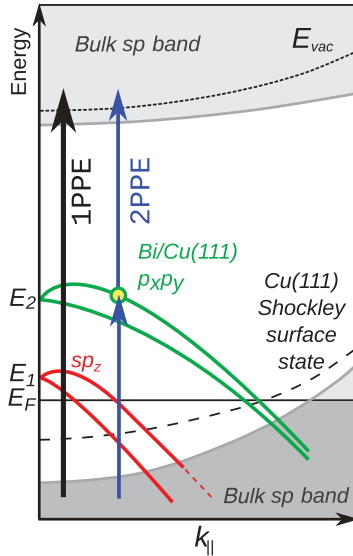


FIG. 1. (Color online) Schematic band structure of Bi/Cu(111), including the Bi-related  $sp_z$  and  $p_x p_y$  surface states with respect to the Cu(111) bulk band structure. The Shockley surface state is observed only at the clean Cu(111) surface. Compared to 1PPE with  $h\nu \approx 6$  eV, 2PPE with  $h\nu \approx 3$  eV is sensitive to intermediate unoccupied states due to the Bi surface alloy as shown by the arrows.  $E_1$  and  $E_2$  indicate the  $\bar{\Gamma}$  energy levels of the Bi-related  $sp_z$  and  $p_x p_y$  states, respectively.  $E_F$  indicates the Fermi level. The vacuum level is at  $E_{vac}$ .

emission patterns between linear and nonlinear photoemission measurements on the Bi/Cu(111) surface. In our case, the unoccupied states favor two-photon transitions, which are related to the Bi surface alloy and, thus, enhance the surface sensitivity of the 2PPE signal in comparison to 1PPE in this specific system. With the help of one-step photoemission calculations, we analyze the polarization dependence of the 2PPE momentum patterns according to the properties of the initial occupied states of the Bi/Cu(111) surface alloy.

## II. EXPERIMENT AND THEORY

We investigate the electronic dispersion of clean Cu(111) and Bi alloys on Cu(111) in the occupied and unoccupied regimes by  $\vec{k}_{\parallel}$ -resolved 1PPE and 2PPE spectroscopies using a momentum microscope.<sup>5</sup> This device has the unique feature that it can directly map the energy-resolved in-plane momentum components  $k_x$  and  $k_y$  of photoelectrons emitted into the full hemisphere ( $\pm 90^\circ$ ) without the need for sample or detector rotation.

The copper surface is prepared by  $Ar^+$ -ion sputtering and annealing under ultrahigh vacuum conditions ( $p < 8 \times 10^{-11}$  mbar). The surface quality was checked by spatial imaging in a photoelectron emission microscope and by the photoemission spectra. Approximately, a 1/3 monolayer<sup>17</sup> of Bi is thermally evaporated on the clean Cu(111) surface at a temperature of 450 K. During the deposition, medium-energy electron diffraction is used for monitoring the growth of the Bi overlayer to obtain a long-range-ordered ( $\sqrt{3} \times \sqrt{3}$ ) $R30^\circ$  surface reconstruction. Following the preparation, all photoemission measurements were performed at 170 K.

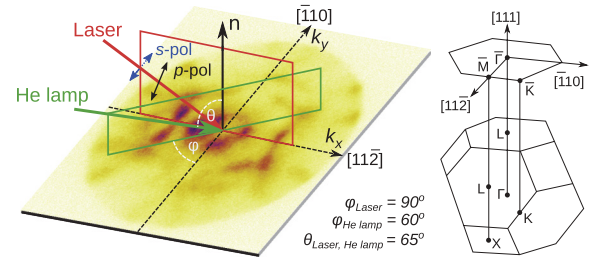


FIG. 2. (Color online) Experimental geometry for photoexcitation by the laser ( $h\nu = 3.1$ ,  $h\nu = 6$  eV) and the He lamp (21.2 eV).  $k_x$  and  $k_y$  are the respective surface-parallel momentum components of the emitted photoelectrons.

Figure 2 illustrates the geometry of our measurements. For reference, the surface Brillouin zone (SBZ) of Cu(111) is shown with indicated high-symmetry directions in relation to the bulk Brillouin zone. In the experimental geometry of the present paper, the crystal is oriented with  $k_x$  parallel to the bulk  $[11\bar{2}]$  direction and  $k_y$  parallel to the  $[\bar{1}10]$  direction. For the 2PPE spectroscopy, the photoelectrons are excited by the second harmonics of a Ti:sapphire femtosecond laser with a photon energy of  $h\nu = 3.1$  eV and a pulse width of about 20 fs. For the 1PPE spectroscopy, either the fourth harmonics of the Ti:sapphire laser with a photon energy of  $h\nu = 6.0$  eV or the He I discharge lamp radiation of photon energy  $h\nu = 21.2$  eV is used. The laser light or the He I radiation are incident from viewports in two different directions.

For the theoretical calculations of both electronic structure and photoemission intensities, we rely on the local density approximation to density functional theory using a relativistic multiple-scattering approach [layer Korringa-Kohn-Rostoker (KKR)]. Solving the Dirac equation, spin-orbit coupling is included. We use the Perdew-Wang exchange-correlation functional.<sup>18</sup> The photoemission spectra from Bi/Cu(111) were computed within the one-step model using self-consistent potentials as input as described by Mirhosseini *et al.*<sup>12</sup>

## III. RESULTS

### A. Fermi-level momentum maps of Cu(111) and Bi/Cu(111) using He I excitation

In Figs. 3(a) and 3(b), we show the momentum maps of the photoemitted intensity  $I(k_x, k_y)$  obtained by unpolarized He I excitation in the vicinity of the Fermi level ( $E_F - 50$  meV) from Cu(111) and Bi/Cu(111), respectively.

For clean Cu(111) (work function  $\Phi = 4.6$  eV) and excitation by He I ( $h\nu = 21.2$  eV), the largest possible electron momentum parallel to the surface is limited by the kinetic energy of photoemitted Fermi-level electrons to about  $2.07 \text{ \AA}^{-1}$ , defining the so-called “photoemission  $k$ -space horizon” for this photon energy. The Shockley surface state of Cu(111) is seen as a circle in the middle of Fig. 3(a). The threefold symmetry of the Cu bulk band structure around the  $[111]$  direction is recognized by the photoemission bulk  $sp$  bands near the boundary of the hexagonal SBZ as seen in the figure. The clean Cu(111) momentum map was recorded in 10 min of integration time and was obtained in an experiment with the Cu crystal rotated by  $30^\circ$  with respect to all other measurements

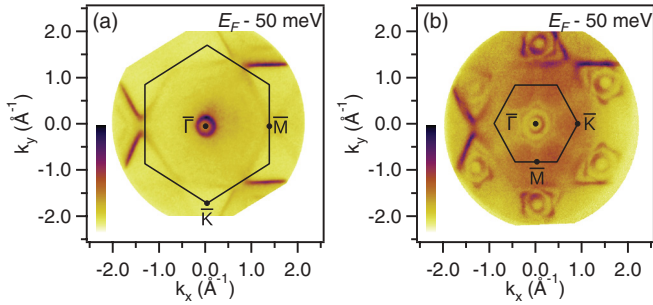


FIG. 3. (Color online) Momentum maps of (a) Cu(111) and (b)  $(\sqrt{3} \times \sqrt{3})R30^\circ$  Bi/Cu(111) as measured by He I radiation. The corresponding surface Brillouin zones are shown by hexagons. The  $k_{\parallel}$ -space periodicity of the electronic structure of the Bi  $(\sqrt{3} \times \sqrt{3})R30^\circ$  superstructure is directly seen in the right pattern by the translated copies of the central structure around  $\bar{\Gamma}$ .

shown in this paper. For a detailed study of the electronic structure of Cu using the momentum microscope, see Ref. 6.

In Fig. 3(b), it is seen that the photoemission horizon is enlarged due to the lower work function of the sample after Bi deposition. Typically, the work function of Cu(111) is reduced by about 0.5 eV after formation of the  $(\sqrt{3} \times \sqrt{3})R30^\circ$  superstructure as judged by the low-energy photoemission threshold measured by laser excitation (see below). A comparison to the clean Cu(111) pattern enables us to distinguish the particular changes which are induced by the Bi surface alloy. First of all, the Bi  $(\sqrt{3} \times \sqrt{3})R30^\circ$  overlayer results in a correspondingly reduced and rotated surface Brillouin zone (as sketched in the figure), which is why the neighboring six Brillouin zones become beautifully visible in the Fermi-level momentum map as translated copies of the central structure in the first SBZ near  $\bar{\Gamma}$ . There, the  $\bar{\Gamma}$  point is surrounded by two concentric circles, which correspond to the Fermi contours of the Rashba-split  $sp_z$  bands shown in Fig. 1. Because the accessible momentum range is comparatively large for He I excitation, the fine structure of the Rashba-split rings is not perfectly visible. However, the momentum maps with higher magnification used in the laser-based experiments can clearly resolve these bands and their dispersions as we see below. The two concentric rings of the Rashba-split Bi surface alloy states near the  $\bar{\Gamma}$  point are furthermore surrounded by a hexagon extending to  $k_x = \pm 0.3 \text{ \AA}^{-1}$ , corresponding to the occupied part of the  $p_x p_y$  states.<sup>13</sup>

Our observations using the He light source verify and extend previous results by the direct mapping of several SBZs and directly visualize the paradigmatic concept of the periodic surface band structure. As we also see in Fig. 3(b), although the geometric shape of the surface-state features repeats itself in different SBZs, the actual photoemission intensities from the Bi surface states are not completely equivalent.<sup>19</sup>

### B. Momentum maps for 1PPE and 2PPE from clean Cu(111)

We now turn to the results of laser-based 1PPE and 2PPE measurements on clean Cu(111) surfaces. The corresponding momentum maps  $I(k_x, k_y)$  at an energy  $E_F - 50 \text{ meV}$  show the Shockley surface state (inner circle) and direct optical

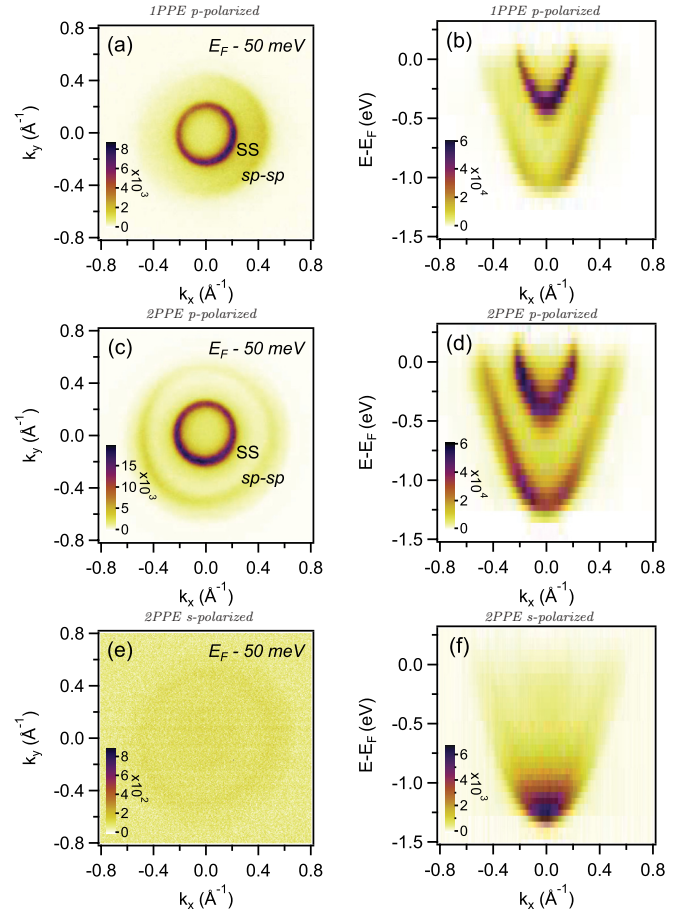


FIG. 4. (Color online) Momentum maps for 1PPE and 2PPE from clean Cu(111) near  $E_F - 50 \text{ meV}$  (left) and the corresponding energy-dependent dispersions for transitions in the plane  $k_y = 0$  (right). (a) and (b) The 1PPE with  $p$ -polarized light, (c) and (d) 2PPE with  $p$ -polarized light, and (e) and (f) 2PPE with  $s$ -polarized light.

$sp$ - $sp$  transitions (outer circle) using  $p$ -polarized light in both 1PPE [Fig. 4(a)] as well as 2PPE [Fig. 4(c)]. The distribution of the direct optical  $sp$ - $sp$  transitions agrees with previous measurements.<sup>20</sup> The slightly larger photoemission horizon in the 2PPE process is due to the 0.2 eV higher total photon energy compared with that of the 1PPE process. This is why, in 2PPE, the outer  $sp$ - $sp$  transition is completely visible as a ring, whereas, in 1PPE, this transition is hidden to a large extent beyond the photoemission horizon. As we will see below, the 1PPE  $sp$ - $sp$  transition will be completely unveiled by the work-function reduction after Bi adsorption. For comparison to the  $p$ -polarized excitation, we show  $s$ -polarized 2PPE measurements in Fig. 4(e). The excitation of surface-state and  $sp$  bands is severely reduced using  $s$ -polarized excitation in both linear and nonlinear photoemission regimes. This is in agreement with selection rule arguments<sup>3</sup> because the  $sp_z$  character of these states does not allow optical transitions by light with electric-field components within the surface plane.

The experimental dispersion relations  $E(\vec{k}_{\parallel})$  corresponding to the complete energy-resolved set of the momentum maps at  $k_y = 0$  are depicted in Figs. 4(b), 4(d), and 4(f). These

cuts correspond to the  $\bar{M}-\bar{\Gamma}-\bar{M}$  direction of the (111) surface. We find the binding energy of the Shockley surface state at 370 meV, and its effective mass is determined to be  $m_{\text{eff}} = 0.4m_e$  for both photoemission regimes.<sup>21</sup> These values agree well with literature values,<sup>22</sup> taking into account temperature effects.

Overall, both 1PPE and 2PPE measurements produce very similar momentum patterns from the clean Cu(111) surface indicating the dominance of the initial and final states in both regimes (see Fig. 1). This is consistent with the fact that there are no unoccupied intermediate states on Cu(111), which are resonantly accessible in 2PPE with the photon energies near 3.1 eV that we use here.

### C. Momentum maps for 1PPE and 2PPE from Bi/Cu(111)

The effect of the  $1/3$ -monolayer Bi adsorption with a surface reconstruction of  $(\sqrt{3} \times \sqrt{3})R30^\circ$  is presented for 1PPE in Fig. 5 and for 2PPE in Fig. 6. We begin with the 1PPE results: Figures 5(a) and 5(c) correspond to 1PPE momentum maps with  $p$ -polarized and  $s$ -polarized laser light, respectively. The corresponding dispersion relations are presented in Figs. 5(b) and 5(d). Additionally, in Fig. 5(e), we present the

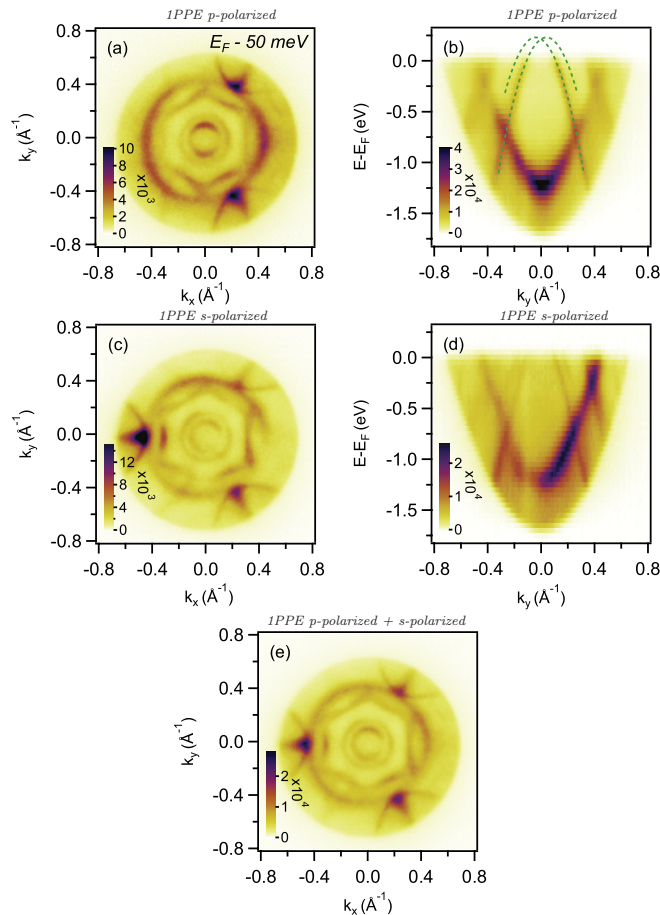


FIG. 5. (Color online) Momentum maps in 1PPE from  $(\sqrt{3} \times \sqrt{3})R30^\circ$  Bi/Cu(111) (left) and the energy-dependent  $k_y$  dispersion for transitions in the plane  $k_x = 0$  (right). (a) and (b)  $p$ -polarized light, (c) and (d)  $s$ -polarized light, and (e) the sum of  $p$ - and  $s$ -polarized measurements.

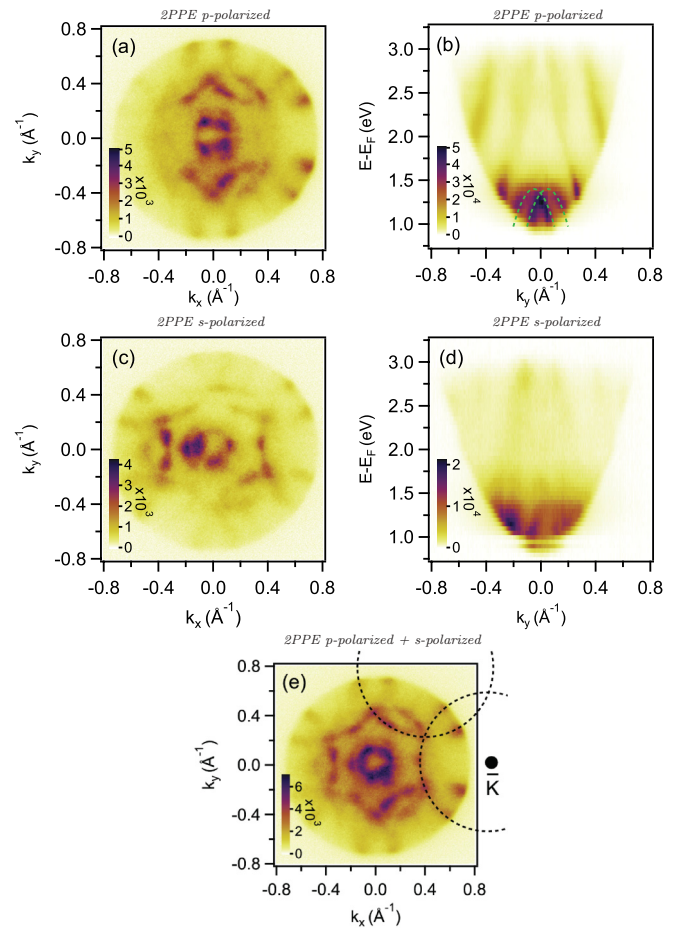


FIG. 6. (Color online) Momentum maps in 2PPE from  $(\sqrt{3} \times \sqrt{3})R30^\circ$  Bi/Cu(111) (left) and the energy-dependent  $k_y$  dispersion for transitions in the plane  $k_x = 0$  (right). (a) and (b)  $p$ -polarized light, (c) and (d)  $s$ -polarized light, and (e) the sum of  $p$ - and  $s$ -polarized measurements with the two indicated circular contours centered at  $\bar{K}$  points of the Bi/Cu(111) surface Brillouin zone.

summed 1PPE momentum maps for both polarizations for the same laser intensity, thus, corresponding to unpolarized excitation.

It has been mentioned above, in Fig. 3(b), for the He I measurements, that the Shockley surface state of Cu(111) is replaced by states induced by the Bi surface alloy. In the He I measurements shown above, the spin splitting of the  $sp_z$  surface states could not be obtained with high resolution due to the enlarged photoemission momentum space. Here, however, Figs. 5(a) and 5(c) display very clearly the concentric rings corresponding to the spin-orbit split states. The hexagonal structure surrounding the two central rings is also seen in the  $p$ - and  $s$ -polarized measurements. Both  $p$  and  $s$  polarizations can excite the Rashba-split rings and the hexagonal feature, showing that these states exhibit intensities that depend both on  $k$  and on the incident polarization.

Apart from the Bi-induced states, the optical transitions resulting from the copper substrate are also clearly visible in the 1PPE measurements of Fig. 5: The ringlike  $sp$ - $sp$  transitions [Fig. 4(c)] surround the Bi bands with threefold additions coming from backfolding of the bulk transition,<sup>23</sup> which is an example of surface umklapp processes.<sup>24,25</sup>

Very interestingly, in the  $p$ -polarized excitation regime, only two of the three contours are seen, and in the  $s$ -polarized excitation regime, all three are visible with the one on the left-hand side having very high intensity. To analyze this polarization-selective issue, we also present the case where  $p$ - and  $s$ -polarized momentum maps are added (leading to the result for unpolarized excitation) in Fig. 5(e). There, it is seen that all three of the backfolded contours as well as the Bi-induced states have equal intensities and result in a pattern with overall threefold rotational symmetry.

Analyzing the dispersion relations of these measurements [Figs. 5(b) and 5(d)], it is seen that the top of the  $sp_z$  bands of the Bi surface alloy is found above  $E_F$ , which is consistent with previous results.<sup>12,13</sup> Due to the photon energy used in the experiment, however, we cannot realize a two-photon transition from  $E_F + 0.1$  eV to above the vacuum level (see Fig. 1), which would be necessary to map the unoccupied part of the  $sp_z$  bands. The occupied parts of these spin split  $sp_z$  surface states can be described by the Rashba model  $E_{\pm}(k_{\parallel}) = E_0 + \frac{\hbar^2}{2m_{\text{eff}}}(k_{\parallel} \pm \Delta k_{\parallel})^2$  (Ref. 13). The effective mass of the surface states is found to be  $-0.37m_e$ , the momentum offset between the band maxima is  $0.08 \pm 0.01 \text{ \AA}^{-1}$ , and the Rashba energy (the energy gap between the crossing point of the bands to their maxima) is determined as 20 meV.

According to the previous theoretical calculations and experimental measurements,<sup>12</sup> there are unoccupied  $p_x p_y$  states located around 1.4 eV above  $E_F$ . The photon energy of 3.1 eV used for 2PPE enables us to map the top part of the unoccupied  $p_x p_y$  bands as sketched in Fig. 1. The corresponding 2PPE results are shown in Fig. 6. Here, for similar initial state energies as for the 1PPE results in Fig. 5, we show momentum maps with  $p$ - and  $s$ -polarized light [Figs. 6(a) and 6(c)] and their corresponding dispersion relations [Figs. 6(b) and 6(d)] side by side. The unpolarized case is shown separately in Fig. 6(e). The Fermi-level momentum maps show transitions from initial states near the Fermi level via intermediate states located one photon energy above. A striking difference between the 1PPE and the 2PPE measurements is the severe suppression of the visibility of the direct optical bulk transitions in 2PPE, which is discussed below. The absence of the  $sp$ - $sp$  bulk transition allows one to see pronounced polarization effects for the surface states in the 2PPE measurements where the Bi-induced features are  $k$ -dependently excited using different polarizations of light. The comparison of Figs. 6(a) and 6(c) with Fig. 6(e) shows that  $p$ -polarized light predominantly excites the states that lie near the  $k_y$  axis and  $s$ -polarized light emphasizes those near the  $k_x$  axis.

The dispersion relations from  $p$ -polarized excitation in Fig. 6(b) show the above-mentioned unoccupied  $p_x p_y$  states as inverted parabolas. They cross at  $k_y = 0$  near  $E = 1.4$  eV, which agrees very well with the theoretical calculations, and the band maxima are offset from each other by about  $0.10 \pm 0.01 \text{ \AA}^{-1}$ . The Rashba energy is measured to be 50 meV, and the effective mass of these surface states is determined to be around  $-0.2m_e$ . There are four additional bands seen at higher energies in the dispersion map of Fig. 6(b). The origin of these bands is the occupied part of the  $sp_z$  states near the Fermi level and below.

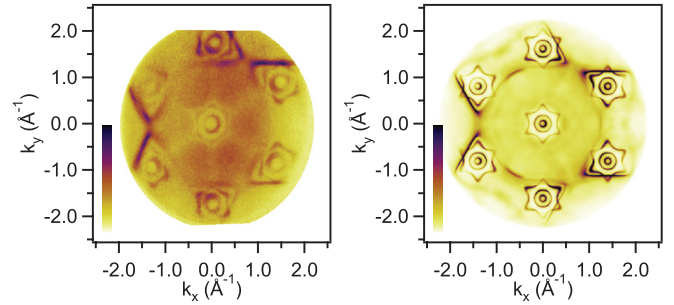


FIG. 7. (Color online) Photoemission from Bi/Cu(111) near the Fermi level. (Left) Experiment He I excitation and (right) one-step photoemission calculation.

## IV. DISCUSSION

In order to test the applicability of one-step photoemission calculations for the interpretation of our measurements, we compare the experimental intensity map at the Fermi level for He I excitation with a calculated intensity distribution as seen in Fig. 7. The qualitative structure of the measured pattern is well reproduced by the calculation. The most obvious quantitative difference is seen in the spin-orbit splitting of the Bi surface alloy states, which is overestimated by the theory. This effect is known also from other KKR calculations.<sup>26</sup>

### A. Polarization dependence

Having in mind the level of agreement of the one-step photoemission calculation for the He I observations, we also simulated the 1PPE measurements with 6 eV photon energy in Fig. 8. The considerably reduced photoemission horizon for this low photon energy leads to emission in the  $k$  range of  $\pm 0.8 \text{ \AA}^{-1}$  and corresponds to the central part of the He lamp measurements in Fig. 7. The main features of the direct  $sp$ - $sp$  transitions and the backfolded structures are nicely reproduced by the theory. Comparison to the experimental data in Fig. 5 shows nice agreement with the experimentally observed polarization dependence of the backfolded  $sp$ - $sp$  transitions. This polarization dependence can be understood from the  $p_z$ -like character of the relevant  $sp$  bands near the  $L$  direction in combination with the projection of the light's polarization vector on the symmetry-equivalent  $L$  directions away from the [111] surface normal.<sup>23</sup> Looking at the Rashba-split states, we see that the spin-orbit splitting is overestimated like before in Fig. 7. Qualitatively, the inner ring shows a higher intensity than the outer one for  $p$ -polarized light. This is consistent with the measurements in Fig. 5(a). For  $s$ -polarized light, only a very low photoemission intensity should be produced from the Rashba-split states compared to the bulk  $sp$ - $sp$  transitions according to the calculation in Fig. 8. We assign the relatively higher intensity of the rings seen in the  $s$ -polarized measurement in Fig. 5(c) to a remaining phase-shifted  $p$ -polarized component in the excitation light, which would also be consistent with the breaking of the mirror symmetry with respect to the horizontal optical plane.

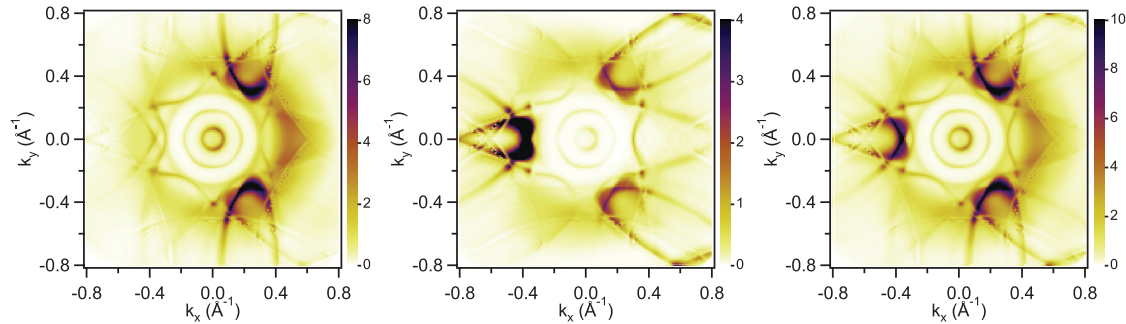


FIG. 8. (Color online) One-step 1PPE calculations for Bi/Cu(111) for photoemission from the Fermi level assuming a final-state optical potential of  $V_{oi} = 0.05$  eV with  $p$ -polarized light (left),  $s$ -polarized light (middle), and the sum of both (right). The characteristic polarization-dependent “chicken-feet” structure of the backfolded direct optical transitions is reproduced, such as observed in the experiments (compare to Fig. 5).

For the analysis of the 2PPE measurements, similar theoretical calculations as for 1PPE are not available at the moment due to the increased complexity of the description of the respective 2PPE processes. For a qualitative discussion of similarities and differences to 1PPE, we resort to simulations of 1PPE with severely broadened bulk transitions. This is achieved by increasing the imaginary part of the crystal potential  $V_{oi}$  (optical potential) for the final states and should qualitatively bring out the influence of the initial surface states. The results in Fig. 9 show a clear difference for  $p$ -polarized light (left) to  $s$ -polarized light (middle) for the hexagonal feature. Similar to what is seen in the experimental 2PPE measurements of Fig. 6, the  $p$ -polarized light emphasizes the tips of the hexagon on the  $k_y$  axis, whereas, the  $s$ -polarized light emphasizes the sides of the hexagon crossing the optical plane. In contrast to this similar behavior in the 2PPE measurements, the 1PPE calculations do not reproduce the node along the optical plane seen for  $p$ -polarized 2PPE in Fig. 6(a). As a similar trend is seen also for the inner ring in the 1PPE experiment in Fig. 5(a), we cannot assign the reason for this disagreement with theory at the moment.

Considering the 2PPE experiments from Bi/Cu(111), in addition to the reduced energy and  $k$  resolution caused by the broad excitation spectrum of the ultrashort excitation pulses, the measurements show a structure with a number of local

peaks instead of the more continuous features seen in the 1PPE experiments. A mechanism that could lead to this structure is the  $k$ -specific enhancement of 2PPE due to resonances with intermediate states. In this case, the structure and symmetry of the  $k$ -dependent initial and intermediate densities of states should directly influence the observed 2PPE intensity. This is why we show, in Fig. 10, the spectral density of states at the Fermi level (left) at one-photon energy above the Fermi level (middle) and the product of both (right). We can see that, in our case, the initial states provide the overall “hexagon + two ring” structure seen in the measurements. Apart from the initial-state structure, the product of the spectral densities relevant for 2PPE is influenced by the intermediate states as we can see, e.g., by local enhancements of intensity along the hexagon, rather similar to what is experimentally observed (Fig. 6).

### B. Relative surface sensitivity of 2PPE and 1PPE

A striking feature of the 2PPE momentum maps is the clear visibility of the direct optical bulk  $sp$ - $sp$  transition on the clean Cu(111) surface, although this bulk feature is severely reduced in the 2PPE measurements from Bi/Cu(111).

Obviously, the presence of unoccupied Bi-related states increases the probability for resonant and nonresonant two-photon transitions in the Bi surface alloy relative to the

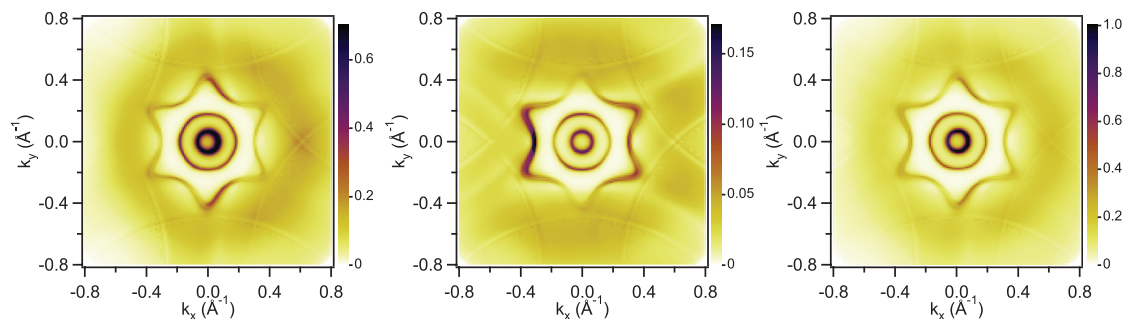


FIG. 9. (Color online) One-step 1PPE calculations for Bi/Cu(111) for photoemission from the Fermi level with an optical potential of  $V_{oi} = 2$  eV in the final state to emphasize polarization effects on the initial states with  $p$ -polarized light (left),  $s$ -polarized light (middle), and the sum of both (right). The hexagonal initial state patterns of the 1PPE ( $h\nu = 6$  eV) calculations resemble the experimental 2PPE ( $2h\nu = 6.2$  eV) patterns (Fig. 6), indicating the dominating influence of the initial states in the respective 2PPE processes.

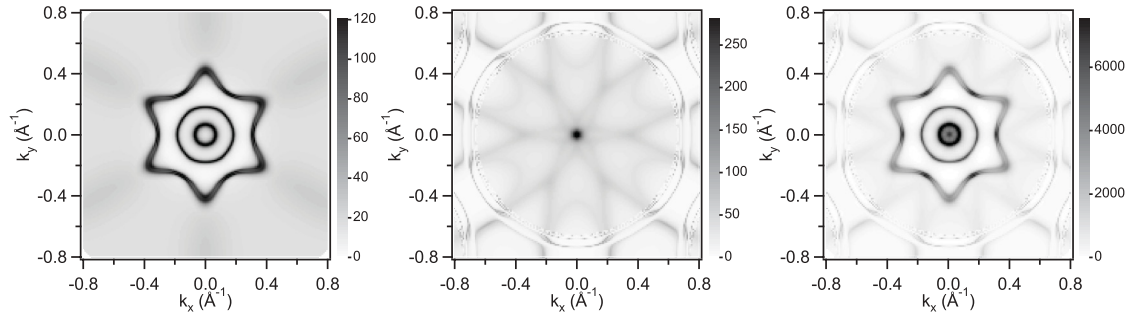


FIG. 10.  $k_{\parallel}$ -resolved spectral density of states relevant for 2PPE from the Bi/Cu(111) surface layer. (Left) Initial states at Fermi level  $E_F$ , (middle) intermediate states at  $E_F + 3$  eV, and (right) the product of initial and intermediate densities of states showing a dominating influence of the initial-state structure.

nonresonant bulk transitions between Cu bulk states. Because the intermediate Bi-related  $p_x p_y$  and  $s p_z$  electronic states are spatially localized in the surface layer of the Cu(111) crystal, this results in a pronounced surface sensitivity of the 2PPE processes observed in the investigated surface-alloy system. Similar effects should be present for unoccupied Bi quantum-well states, which are observed when the amount of deposited Bi is increased.<sup>27</sup> Compared to the 2PPE process, the additional unoccupied states are not relevant for one-photon transitions, which explains the relatively constant 1PPE contribution of the direct optical bulk transitions from both Bi/Cu(111) and clean Cu(111). The thickness region sampled by the 1PPE is on the order of the inelastic mean-free path at the final-state energy and comprises a significant number of Cu layers on the order of 20 Å.<sup>28</sup>

Specifically, for Bi/Cu(111), the surface localization of the 2PPE process allows for selectively enhancing the Bi surface-alloy states with respect to the Cu(111) bulk crystal states. This can be seen in the 2PPE results of Fig. 6(e) where the dashed circles show how the central hexagonal feature is created by an intersection of six circles, which are, however, of severely reduced intensity outside the actual hexagon. The origins of the circular features are the six symmetry-equivalent  $\bar{K}$  points of the Bi-surface alloy Brillouin zone as can be seen by comparison to Fig. 3. For comparison, in the measurements with the He I source in Fig. 3 as well as in the results using 6 eV photons in Fig. 5, the weaker circular features extending from the central hexagon are absent. This is due to the averaging of bulk and surface signals in these 1PPE measurements where a small surface contribution is overwhelmed by the bulk signal. The intensity reduction in the low-symmetry directions outside the central hexagon seems to be connected to the underlying Cu(111) bulk continuum. The surface-alloy states in the region of larger  $k_{\parallel}$  couple stronger to the underlying bulk states compared to the positions in the central hexagon, which still are nearer to the band-gap region around  $\bar{\Gamma}$  in the center of Fig. 6(e).

In comparison to the enhancement of the surface electronic structure in 2PPE from Bi/Cu(111), it is important to note that we have recently demonstrated the opposite behavior for photoemission from ultrathin Co films on Cu(001).<sup>29</sup> There, the contribution of an occupied surface resonance is suppressed due to the availability of additional unoccupied quantum-well states for two-photon transitions. In spin-

resolved measurements, we have shown that this scenario favors 2PPE transitions inside the Co film compared to an enhancement of the surface contribution in 1PPE. Thus, the measurements presented in this paper and those in Ref. 29 show that the problem of the relative surface sensitivity of 1PPE vs 2PPE cannot be discussed without consideration of the depth-resolved electronic structure of the specific system under study. As an application, we suggest that going from 1PPE with a one-photon excitation energy of  $h\nu$  to a two-photon excitation with  $h\nu/2$  provides a way to tune the surface sensitivity of the observed photoemission signal, which can be exploited in future studies.

## V. SUMMARY

We investigated the polarization dependence of photoelectron momentum maps in linear and nonlinear photoemission measurements from clean Cu(111) and from the long-range-ordered  $(\sqrt{3} \times \sqrt{3})R30^\circ$  surface reconstruction of a Bi/Cu(111) surface alloy. In the case of clean Cu(111), 1PPE and 2PPE measurements both showed similar photoemission momentum patterns and a similar polarization dependence as a result of direct optical transitions from the occupied initial states to the final states. In contrast to the clean Cu(111) surface, very different emission patterns were observed from Bi/Cu(111) in  $p$ -polarized and  $s$ -polarized 1PPE and 2PPE measurements. The 1PPE experiments on this system showed a polarization dependence in the form of appearance or suppression of photoemission intensity of the backfolded  $sp$ - $sp$  transitions, which we assigned to the  $p_z$ -like character of the relevant  $sp$  bands near the  $L$  direction by using one-step photoemission calculations. Similarly, we found that the presence of unoccupied states on Bi/Cu(111) emphasized surface two-photon transitions specific to the Bi alloy as compared to the bulk contributions seen in 1PPE. We argued that the polarization dependence of 2PPE momentum patterns of Bi/Cu(111) stemmed from the properties of its occupied initial states and was additionally influenced by the unoccupied intermediate states. The experimental investigation using our momentum microscope provided comprehensive information on the polarization dependence of the  $k$ -resolved photoemission features of Bi/Cu(111). We suggested a way to tune the surface sensitivity of an observed photoemission signal by switching between one-photon and two-photon excitations.

- <sup>1</sup>*Angle-Resolved Photoemission, Theory and Current Applications*, edited by S. D. Kevan (Elsevier, Amsterdam, 1992).
- <sup>2</sup>S. Hüfner, *Photoelectron Spectroscopy*, 3rd ed. (Springer-Verlag, Berlin/Heidelberg/New York, 2003).
- <sup>3</sup>J. Hermanson, *Solid State Commun.* **22**, 9 (1977).
- <sup>4</sup>W. Eberhardt and F. J. Himpsel, *Phys. Rev. B* **21**, 5572 (1980).
- <sup>5</sup>B. Krömker, M. Escher, D. Funnemann, D. Hartung, H. Engelhard, and J. Kirschner, *Rev. Sci. Instrum.* **79**, 053702 (2008).
- <sup>6</sup>A. Winkelmann, C. Tusche, A. A. Ünal, M. Ellguth, J. Henk, and J. Kirschner, *New J. Phys.* **14**, 043009 (2012).
- <sup>7</sup>J. D. Koralek, J. F. Douglas, N. C. Plumb, J. D. Griffith, S. T. Cundiff, H. C. Kapteyn, M. M. Murnane, and D. S. Dessau, *Rev. Sci. Instrum.* **78**, 053905 (2007).
- <sup>8</sup>G. Liu, G. Wang, Y. Zhu, H. Zhang, G. Zhang, X. Wang, Y. Zhou, W. Zhang, H. Liu, L. Zhao, J. Meng, X. Dong, C. Chen, Z. Xu, and X. J. Zhou, *Rev. Sci. Instrum.* **79**, 023105 (2008).
- <sup>9</sup>T. Kiss, T. Shimojima, K. Ishizaka, A. Chainani, T. Togashi, T. Kanai, X.-Y. Wang, C.-T. Chen, S. Watanabe, and S. Shin, *Rev. Sci. Instrum.* **79**, 023106 (2008).
- <sup>10</sup>C. R. Ast, J. Henk, A. Ernst, L. Moreschini, M. C. Falub, D. Pacilé, P. Bruno, K. Kern, and M. Grioni, *Phys. Rev. Lett.* **98**, 186807 (2007).
- <sup>11</sup>J. H. Dil, *J. Phys.: Condens. Matter* **21**, 403001 (2009).
- <sup>12</sup>H. Mirhosseini, J. Henk, A. Ernst, S. Ostanin, C.-T. Chiang, P. Yu, A. Winkelmann, and J. Kirschner, *Phys. Rev. B* **79**, 245428 (2009).
- <sup>13</sup>H. Bentmann, F. Forster, G. Bihlmayer, E. V. Chulkov, L. Moreschini, M. Grioni, and F. Reinert, *EPL* **87**, 37003 (2009).
- <sup>14</sup>C. R. Ast, D. Pacilé, L. Moreschini, M. C. Falub, M. Papagno, K. Kern, M. Grioni, J. Henk, A. Ernst, S. Ostanin, and P. Bruno, *Phys. Rev. B* **77**, 081407 (2008).
- <sup>15</sup>L. Moreschini, A. Bendounan, H. Bentmann, M. Assig, K. Kern, F. Reinert, J. Henk, C. R. Ast, and M. Grioni, *Phys. Rev. B* **80**, 035438 (2009).
- <sup>16</sup>E. Frantzeskakis and M. Grioni, *Phys. Rev. B* **84**, 155453 (2011).
- <sup>17</sup>D. Kaminski, P. Poodt, E. Aret, N. Radenovic, and E. Vlieg, *Surf. Sci.* **575**, 233 (2005).
- <sup>18</sup>J. Henk, in *Handbook of Thin Film Materials, Volume 2: Characterization and Spectroscopy of Thin Films*, edited by H. S. Nalwa (Academic, San Diego, 2002), Chap. 10, pp. 479–526.
- <sup>19</sup>D.-W. Lee and C. Kim, *J. Anal. Sci. Technol.* **1**, 118 (2010).
- <sup>20</sup>M. Hengsberger, F. Baumberger, H. J. Neff, T. Greber, and J. Osterwalder, *Phys. Rev. B* **77**, 085425 (2008).
- <sup>21</sup>A. A. Ünal, C. Tusche, S. Ouazi, S. Wedekind, C.-T. Chiang, A. Winkelmann, D. Sander, J. Henk, and J. Kirschner, *Phys. Rev. B* **84**, 073107 (2011).
- <sup>22</sup>F. Reinert, G. Nicolay, S. Schmidt, D. Ehm, and S. Hüfner, *Phys. Rev. B* **63**, 115415 (2001).
- <sup>23</sup>A. Winkelmann, A. A. Ünal, C. Tusche, M. Ellguth, C.-T. Chiang, and J. Kirschner, *New J. Phys.* **14**, 083027 (2012).
- <sup>24</sup>J. Anderson and G. Lapeyre, *Phys. Rev. Lett.* **36**, 376 (1976).
- <sup>25</sup>G. Paolucci, K. C. Prince, B. E. Hayden, P. J. Davie, and A. M. Bradshaw, *Solid State Commun.* **52**, 937 (1984).
- <sup>26</sup>A. Nuber, J. Braun, F. Forster, J. Minár, F. Reinert, and H. Ebert, *Phys. Rev. B* **83**, 165401 (2011).
- <sup>27</sup>S. Mathias, A. Ruffing, F. Deicke, M. Wiesenmayer, I. Sakar, G. Bihlmayer, E. V. Chulkov, Y. M. Koroteev, P. M. Echenique, M. Bauer, and M. Aeschlimann, *Phys. Rev. Lett.* **104**, 066802 (2010).
- <sup>28</sup>W. Krolikowski and W. Spicer, *Phys. Rev.* **185**, 882 (1969).
- <sup>29</sup>C.-T. Chiang, A. Winkelmann, J. Henk, F. Bisio, and J. Kirschner, *Phys. Rev. B* **85**, 165137 (2012).